

# Modeling and Design of a Semi-Integrated QEPAS Sensor

Martino De Carlo , Giansergio Menduni, Angelo Sampaolo , Francesco De Leonardis , Vincenzo Spagnolo, and Vittorio M. N. Passaro , *Senior Member, IEEE*

**Abstract**—Quartz enhanced photo acoustic spectroscopy (QEPAS) has gained a growing interest in recent years for gas sensing technology because of the high sensitivity provided by sharp resonant tuning forks (QTFs) exploited as piezoelectric sound wave detectors; and the modularity, compactness, and robustness of the sensors. The currently used experimental configurations of the QEPAS sensors still rely on free space optics, which are potentially subject to misalignment and require a relatively high space occupation. Here we propose the modelling and the design of a QEPAS sensor with the laser source and optical components for beam delivery bonded together and semi-integrated with the tuning fork. In particular, we propose a configuration in which an optical resonator placed between the prongs of the QTF is coupled with the laser source through a waveguide (OMRSI-QEPAS). For this setup design, COMSOL simulations provided pressure values of the acoustic wavefront comparable with the standard on-beam configuration employing acoustic resonator tubes. Therefore, the design here proposed aims to package the opto-acoustic core of a QEPAS sensor in a single module of few cubic centimeters to definitively address the misalignment issues and pave the way to a further level of miniaturization, integration and deployment for application like mobile and on-drone sensing.

**Index Terms**—Guided-wave devices, integrated optics, photoacoustic spectroscopy, QEPAS, ring resonators.

## I. INTRODUCTION

**P**HOTOACOUSTIC spectroscopy (PAS) is an indirect absorption spectroscopy based on the photoacoustic effect

Manuscript received May 21, 2020; revised September 8, 2020; accepted October 6, 2020. Date of publication October 13, 2020; date of current version January 15, 2021. This work was supported in part by Fondo di Ricerca di Ateneo, Politecnico di Bari. Angelo Sampaolo and Vincenzo Spagnolo were supported by the European Union's Horizon 2020 research and innovation programme under the Marie Skłodowska-Curie project OPTAPHI, under Grant 860808 and from THORLABS GmbH within the joint-research laboratory. (Corresponding author Martino De Carlo.)

Martino De Carlo and Giansergio Menduni are with Photonics Research Group, Department of Electrical and Information Engineering, Politecnico di Bari, 70126 Bari, Italy (e-mail: martino.decarlo@poliba.it; giansergio.menduni@poliba.it).

Francesco De Leonardis and Vittorio M. N. Passaro are with Photonics Research Group, Department of Electrical and Information Engineering, Politecnico di Bari, 70126 Bari, Italy, and also with Institute for Photonics and Nanotechnologies (CNR-IFN), Department of Physics, Politecnico di Bari, 70126 Bari, Italy (e-mail: francesco.deleonardis@poliba.it; vittorio.passaro@poliba.it).

Angelo Sampaolo and Vincenzo Spagnolo are with PolySense Lab, Physics Department, Politecnico and University of Bari, CNR-IFN, 70126 Bari, Italy (e-mail: angelo.sampaolo@poliba.it; vincenzoluigi.spagnolo@poliba.it).

Color versions of one or more of the figures in this article are available online at <https://ieeexplore.ieee.org>.

Digital Object Identifier 10.1109/JLT.2020.3030682

and typically using lasers as excitation sources [1]. When light at a specific wavelength is absorbed by the gas sample, the excited molecules will subsequently relax to the ground state either through emission of photons or by means of non-radiative processes. These processes produce localized heating in the gas, which in turn results in an increase of the local pressure. If the incident light intensity is modulated, the generation of thermal energy in the sample will also be periodic and a pressure wave, *i.e.*, a sound wave, will be produced at the same frequency of the light modulation. The PAS signal can be amplified by tuning the modulation frequency to one of the acoustic resonances of the gas sample cell [2]. The key advantage of this technique is that optical detector is not required, and the resulting sound waves can be detected by a commercial hearing aid microphone. The latest evolution of the PAS technique is Quartz-Enhanced Photoacoustic Spectroscopy (QEPAS), which employ quartz tuning forks (QTF) as core sensitive element [3]. The QTF acts as a sharp resonator and piezoelectric transducer at the same time. The use of QTFs has elevated the QEPAS technique to the best candidate for in-situ and real-time trace gas detection, because of an unmatched level of compactness, extremely high sensitivity (down to ppt), immunity to environmental noise and numerous possibilities of development and upgrade of this technique [4]. QTFs are employed in different applications fields and in most of the case are used for timing and sensing aims. Their main features are: i) resonance frequencies typically falling in the kHz-MHz range, depending on prongs dimensions and quartz crystal properties; ii) high frequency stability of these resonances, with frequency shifts approximately of  $0.04 \text{ ppm}/(^{\circ}\text{C})^2$  over a wide temperature range, from  $-40^{\circ}\text{C}$  to  $90^{\circ}\text{C}$ ; iii) high quality factors, of few tens of thousands in air at the atmospheric pressure; iv) QTFs have a low cost and small size, thus enabling mass-production [5]. Until 2013, all QEPAS sensors reported in literature made use of QTFs designed for timing applications to vibrate at a resonance frequency of  $32,768 (2^{15}) \text{ Hz}$ . The two prongs of these QTFs are typically 3 mm long, 0.35 mm wide and 0.34 mm thick and are separated by a gap of 0.3 mm. They have a quality factor as high as 30,000 in air, increasing up to 100,000 in vacuum [3]. In QEPAS, to increase the effective interaction length between the radiation-generated sound and the QTF, an acoustic resonator is also usually installed. The acoustic system composed of the QTF and the acoustic resonator is referred as QEPAS spectrophone. The resonators used so far consist of two metallic tubes aligned perpendicular to the QTF plane (on beam-QEPAS) [6], parallel to the QTF plane (off-beam

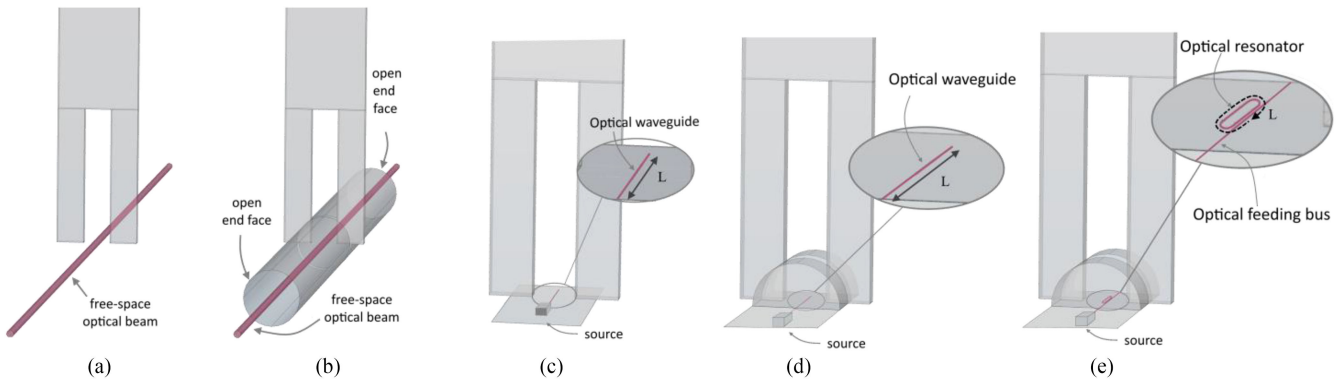


Fig. 1. Different configurations of QEPAS setups analyzed in this work. FS-QEPAS (a) is a simple QEPAS configuration without any mechanical resonator. MR-QEPAS (b) is a free space configuration with a mechanical resonator. SI-QEPAS (c) is a semi-integrated version of QEPAS without mechanical resonators. MRSI-QEPAS (d) is a semi-integrated version of QEPAS with a mechanical resonator. OMRSI-QEPAS (e) is a semi integrated version of QEPAS with a mechanical resonator and an optical resonator (fed by an optical bus).

QEPAS) [7] or one single tube placed between the QTF prongs with a pair of small slits in correspondence of the pressure maximum [8].

One of the main issues with QEPAS based sensor systems is the required focusing of the laser excitation beam between the QTF prongs. The laser beam must not hit the prongs since otherwise a large undesirable non-zero background arises due to the laser contribution, hence limiting the sensor detection sensitivity [9]. This problem triggered several solutions, for instance the use of the Hollow Core Waveguides (HCW) to be coupled with the laser sources for guiding the light and clean up the laser beam mode profile [10]–[12].

The short optical pathlength, the capability to reach high detection sensitivity, high compactness and robustness represent the main distinct advantages which made QEPAS the leading-edge technique mature for out-of-laboratory operation, targeting in-situ applications such as environmental monitoring and leak detection [13], [14]. Nevertheless, for those applications in which sensors must work in challenging environments like downhole analysis of natural gas or early fire detection empowered by the drone technology, the further miniaturization step requires a different level of integration of the opto-acoustic components [15]–[18]. The approach we propose in this work is meant to exploit the enhancement of light provided by resonant cavities together with a mechanical microresonator to make the performances of a semi-integrated QEPAS sensor comparable with those obtained in free space. The integration of a laser source on Silicon chips is today possible thanks to bonding processes [19]. Therefore, the possibility of integrating all the optical components of a QEPAS system on a Silicon chip, apart from the QTF, could represent a promising alternative. Due to some limitations of integrated waveguides, such as a small confinement factor on cladding [20], it is not easy to achieve performances comparable to the state-of-art QEPAS. Thus, a feasibility study on semi-integrated versions of QEPAS setups will be here presented and supported by numerical simulation in COMSOL Multiphysics.

In this paper five different configurations, schematically depicted in Fig. 1, will be investigated and compared:

- FS-QEPAS (Free Space QEPAS): standard configuration without mechanical resonators
- MR-QEPAS (Mechanical Resonator QEPAS): a free space configuration using a mechanical microresonator to enhance the pressure signal (state-of-art)
- SI-QEPAS (Semi-Integrated QEPAS): semi-integrated version without mechanical resonators
- MRSI-QEPAS: (Mechanical Resonator, Semi-Integrated QEPAS): semi-integrated version with a mechanical resonator
- OMRSI-QEPAS: (Optical and Mechanical Resonators, Semi-Integrated QEPAS): semi-integrated version with a mechanical resonator and an optical resonator

## II. MACROSCOPIC MODELING OF PHOTOACOUSTIC WAVE GENERATION

In photoacoustic spectroscopy, as well as in QEPAS, the signal  $S$  obtained from the acoustic-electrical transducer, *i.e.* the microphone or the tuning fork, is proportional to the absorption coefficient  $\alpha$  of the gas sample, the radiation-to-sound conversion efficiency  $\varepsilon$ , the QTF quality factor  $Q$  and the optical power  $P$  available from the laser source [4]:

$$S \approx \alpha Q P \varepsilon \quad (1)$$

In order to design a semi-integrated version of the QEPAS sensor with performances comparable with the standard QEPAS systems, we initially try to model the soundwave generated by photoacoustic effect starting from the fraction of optical power interacting with the target gas. The light absorbed by the gas is converted into a heat source ( $H$ ) proportional to the absorbed optical intensity  $I$  [21]

$$H(\vec{r}, t) = \alpha I(\vec{r}, t) \quad (2)$$

where  $\alpha$  is the power absorption coefficient per unit length. The generated heat  $H$  and the consequent energy relaxation gives rise to acoustic waves. The Helmholtz equation in the harmonic regime can be written as follows [1]:

$$\left( \nabla^2 + \frac{\omega^2}{v^2} \right) p(\vec{r}, \omega) = -\frac{\gamma - 1}{v^2} j\omega H(\vec{r}, \omega) \quad (3)$$

where  $p$  is the local pressure,  $v$  is the local speed of sound,  $\gamma$  is the ratio between the specific heat at constant volume ( $C_V$ ) and the specific heat at constant pressure ( $C_P$ ) and  $\omega$  is the angular frequency of the laser excitation.

The solutions of the wave equations are determined by the boundary conditions. In particular, the solution  $p$  can be expressed as an expansion over the modes  $p_j$  with amplitudes  $A_j$  [1]:

$$p(\vec{r}, \omega) = \sum p_j(\vec{r}) A_j(\omega) \quad (4)$$

It can be found that under rigid-walls boundary conditions (good approximation for the boundary condition of microresonators) [1]:

$$A_j(\omega) = \frac{-j\omega^2}{\omega_j} \frac{[(\gamma-1)/V_C] \int p_j^* H dV}{1 - \frac{\omega^2}{\omega_j^2} - j\frac{\omega}{\omega_j Q_j}} \quad (5)$$

where  $\omega_j$  is the resonance angular frequency of the  $j$ -th mechanical resonant mode,  $Q_j$  is the quality factor of the  $j$ -th mode,  $V_C$  is the volume defined by the boundary conditions.

By approximating  $H$  as a two-dimensional Dirac-delta input for the Helmholtz equation (possible if the linear dimensions of the cross-section of the beam are much smaller than the acoustic wavelength) and by considering  $z$  the direction of propagation of the light beam we obtain:

$$H(\vec{r}, t) = \alpha P_{gas} \delta(x, y) \quad (6)$$

with  $P_{gas}$  the fraction of the optical power interacting with the target gas. Thus, eq (5) becomes:

$$A_j(\omega) = \frac{-j\omega^2}{\omega_j} \frac{[(\gamma-1)/S_C] p_j^*(0, 0, z) \alpha P_{gas}}{1 - \frac{\omega^2}{\omega_j^2} - j\frac{\omega}{\omega_j Q_j}} \quad (7)$$

with  $S_C$  the area of the cross section delimited by the boundary conditions. Using Eq. 4:

$$p = \sum p_j A_j = \alpha P_{gas} \sum \frac{-j\omega^2 [(\gamma-1)/S_C] p_j^*(0, 0, z)}{\omega_j \left(1 - \frac{\omega^2}{\omega_j^2} - j\frac{\omega}{\omega_j Q_j}\right)} p_j(\vec{r}) \quad (8)$$

So, we obtained that the amplitude of the pressure, and thus the QTF signal is proportional to the optical power interacting with the target gas ( $P_{gas}$ ).

In free space, all the power of the laser interacts with air, whereas in integrated optical devices, the light is guided into a medium, thus, only a small fraction of the power propagates outside the guide as an evanescent wave and interacts with the gas. The air confinement factor ( $\Gamma_{gas}$ ) is defined as the fraction of the power propagating in air ( $P_{gas}$ ) divided by the total power propagating through the waveguide ( $P_P$ ):

$$\Gamma_{gas} = \frac{\int_{gas} S_z d\vec{S}}{\int_{total} S_z d\vec{S}} = \frac{P_{gas}}{P_P} \quad (9)$$

with  $S_z$  the Poynting vector along the direction of propagation  $z$ .

It means that with the same amount of power consumption and under the same boundary conditions, the pressure amplitude  $p$  of the sound wave, photoacoustically generated by the evanescent

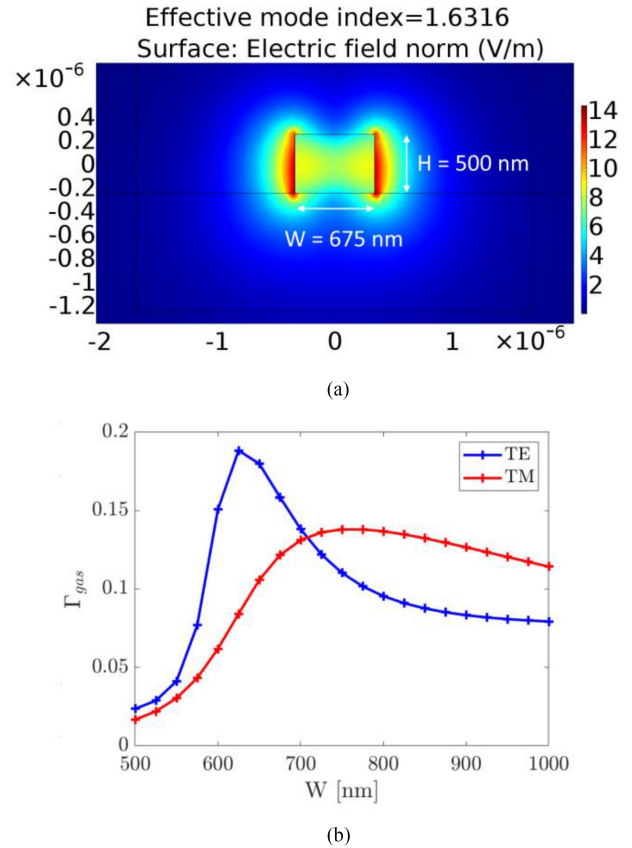


Fig. 2. Light mode in waveguide-based structure for a waveguide width  $W = 600$  nm and height  $H = 500$  nm (a) and Confinement Factor  $\Gamma_{gas}$  for different values of the widths of the waveguide (with  $H = 500$  nm) for TE and TM modes (b).

wave in waveguide-based structure, is  $\Gamma_{gas}$  times lower than the wavefront pressure generated in free space.

Fig. 2(b) shows  $\Gamma_{gas}$  as a function of the width  $W$  of a Silicon waveguide (for a standard waveguide height of 500 nm) for a propagating radiation with a wavelength  $\lambda = 3345$  nm, useful for detecting methane and ethane in the mid-IR region [17]. As it can be seen, the maximum achievable confinement factor is around 18% for this kind of strip waveguides (Fig. 2(b)).

We considered that the dominant source of loss for this waveguide is due to the bulk loss in  $\text{SiO}_2$  (10 dB/cm at a wavelength of  $3.345 \mu\text{m}$  [22]). Consequently, the optimal waveguide design for this application is a trade-off between the fraction of evanescent power in air ( $\Gamma_{gas}$ ) and the total loss of the waveguide. We chose a width of 675 nm, for which the fraction of power in  $\text{SiO}_2$  is 27%, meaning a total propagation loss of 2.7 dB/cm (propagation loss in Silicon is negligible).

Fig. 2(a) shows the designed waveguide (500 nm x 675 nm) and the chosen mode (TE) that will be used for all the integrated configurations in the next sections.

### III. PERFORMANCE COMPARISON: FS-QEPAS VS SI-QEPAS

The key idea of this paper is to demonstrate that a semi-integrated configuration of a QEPAS setup can potentially replace the standard free-space configuration making the space

occupation much lower and eliminating any optical alignment issue. As a first step, we simulated the photoacoustic generation when a free-space laser beam propagates between the prongs of a bare QTF (FS-QEPAS, Fig. 1(a)), which represents a non-interactive element in the following analysis. Then, we compared the FS-QEPAS model with a similar structure exploiting an integrated waveguide on a Silicon chip (SI-QEPAS, Fig. 1(c)). We performed the fully mechanical simulations by implementing the Helmholtz equation (Eq. 3) on the “Pressure Acoustic, Frequency Domain” module of COMSOL Multiphysics, with the heat source  $H$  obtained by combining Eq. 6 and Eq. 9. The wavelength selected is resonant with an optical transition related to the C-H bond stretching of methane at  $2989\text{ cm}^{-1}$  (3345 nm) and having an absorption coefficient of  $\alpha\ 12\text{ cm}^{-1}$  at a pressure of 1 atm and a temperature of 296 K [23].

The QTF selected as a reference to model the non-interacting probe in our design is a tuning fork having a resonance frequency of 15.8 kHz, a prong thickness of  $250\ \mu\text{m}$ , a prong spacing of  $800\ \mu\text{m}$  and thus slightly different from the one investigated in ref [24], which has an enlarged prong spacing of 1.5 mm. The other dimensions of the QTF have no influence on the simulations, because the prong internal surfaces were treated as hard wall boundary conditions. We used an implementation of Helmholtz equation in COMSOL Multiphysics to simulate the pressure signal generated from a heat source located between the free ends of the QTF. In fact, the QTF is aligned so that the light beam propagates perpendicular to the QTF plane and exactly centered between the top of the prongs, where the vibrational antinode is theoretically expected [3]. In the FS-QEPAS case, the light beam has been simulated with an equivalent  $100\ \mu\text{m}$  radius uniform power beam, whereas in the SI-QEPAS case, the light propagates into a waveguide on the surface of an integrated chip (TE mode of a  $675\text{ nm} \times 500\text{ nm}$  Silicon strip waveguide in Fig. 2(a)) and has been simulated with an equivalent  $0.5\ \mu\text{m}$ -radius uniform beam with equivalent power equal to  $P_P \Gamma_{gas}$ . The length of the waveguide has been varied between  $400\ \mu\text{m}$  and 1 mm. For these lengths, the propagation losses due to  $\text{SiO}_2$  have not been accounted into simulation, because negligible.

In both cases a total input power  $P_P = 1\text{ mW}$  was considered. Fig. 3(a) shows the pressure signal in static conditions (for non-vibrating prongs) for a waveguide length  $L$  of 1 mm.

It is easy to appreciate that for the SI-QEPAS configuration, the pressure signal in the proximity of the prongs is almost one order of magnitude lower than in FS-QEPAS case.

#### IV. PERFORMANCES COMPARISON WITH MICRORESONATORS: MR-QEPAS VS MRSI-QEPAS

The employment of acoustic resonator tubes has been widely exploited in literature and in sensor prototypes to increase the SNR of the piezoelectric signal. In the on-beam configuration, a pair of tubes are aligned perpendicular to the QTF plane, with the tube axes at the same height of the fundamental vibration mode antinode and at a distance from the QTF typically of several tens of micron [6]. Thus, when the modulated laser radiation propagates through the dual tube system, a standing soundwave

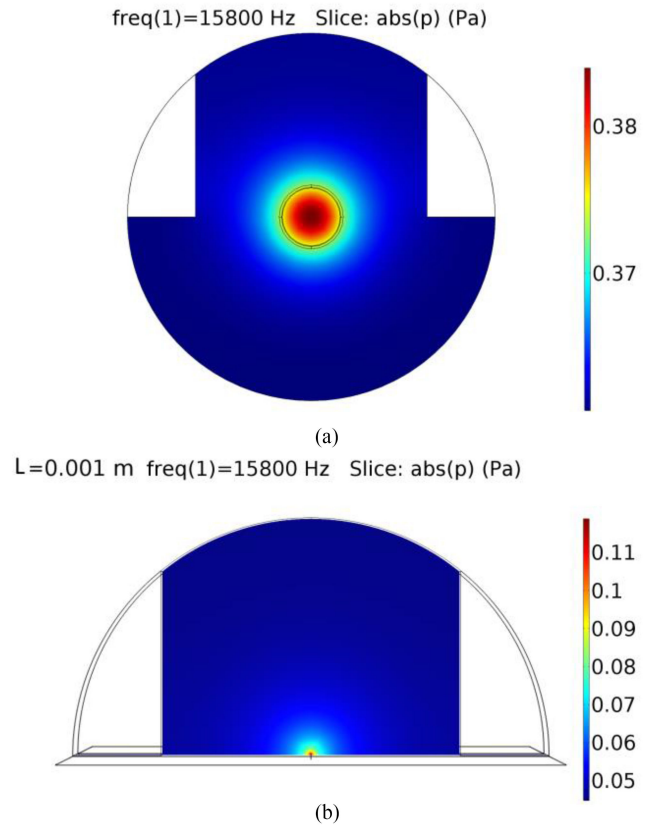


Fig. 3. Acoustic pressure field, with optical power of 1mW without resonators in FS-QEPAS configuration (a) and SI-QEPAS configuration (b).

is photoacoustically generated, with its pressure peak occurring at the vibrational antinode between the prongs. The schematic of the dual tube on-beam configuration, here referred as MR-QEPAS, is shown in Fig. 1(b). acting as a micromechanical resonator enhancing the pressure of the photoacoustic soundwave. This is the most used QEPAS configuration [6]. The MR-QEPAS simulated for this investigation is composed of a cylindrical microresonator open at its end faces. The distance between the internal edges of the tubes was set to  $310\ \mu\text{m}$  to accommodate a QTF for sensing the pressure variations. Each tube is 10.3 mm long, with an inner diameter of 1.27 mm. These tube dimensions demonstrated to provide the highest SNR when acoustically coupled with a 15 kHz custom QTF [24].

The MR-QEPAS was then compared to a SI-QEPAS configuration in which a closed micromechanical resonator was added in order to obtain a further enhancement of the pressure in the proximity of the QTF prongs. The micromechanical resonator is made up of a closed semicylinder with a central gap where the QTF is located. If the laser radiation is delivered through the micro mechanical resonator by means of a feeding bus, the light can be coupled again to the waveguide so that the  $\Gamma_{gas}$  portion of the input power can interact with the target gas over a length  $L$  (Fig. 1(d), MRSI-QEPAS). The size of the gap at the center of the microresonator is the same as in the MR-QEPAS). The inner diameter of the semicylindrical resonator is 1.27 mm and the total microresonator length is 2 mm.

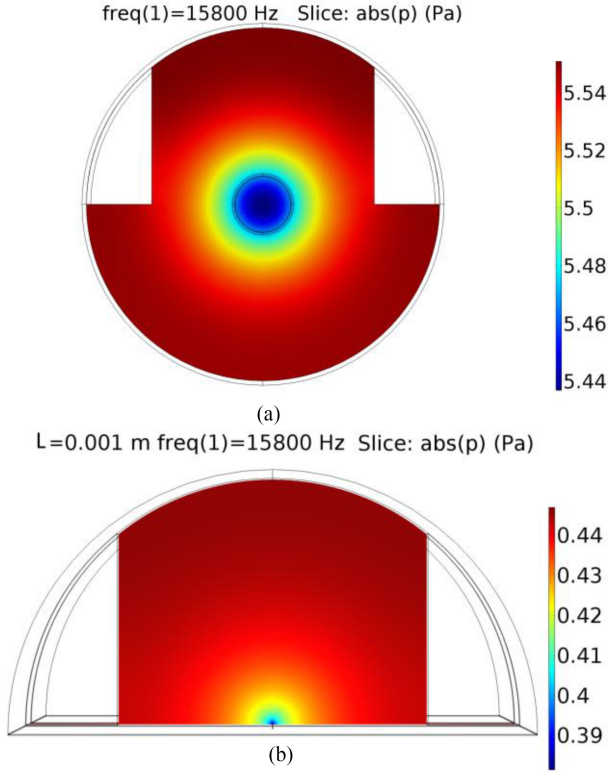


Fig. 4. Acoustic pressure field, with optical power of 1mW without resonators in the MRQEPAS configuration (a) and MRSI-QEPAS configuration (b).

We simulated and compared the pressure signal per input power obtained at the base of the QTF prongs between the MR-QEPAS and the semi-integrated version MRSI-QEPAS. The light beams were simulated as indicated in the previous paragraph. The colormaps in Figs. 4(a) and 4(b) show the pressure signal for input power of 1 mW on the central cross-section for both the configurations (with  $L = 1$  mm in the MRSI-QEPAS case).

In the case of MRSI-QEPAS, since the system is closed, all the optical power absorbed should be converted into a pressure signal. Through an energetic approach it is possible to find the dependence of the pressure signal on the length of the absorption path in the MRSI-QEPAS (approximation of closed system). In particular, when considering an optical mode propagating in an integrated waveguide, the fraction ( $P_{abs,int}$ ) of the total power propagating in the waveguide ( $P_P$ ) that has been absorbed by the target gas over a length  $L$  (in the hypothesis of small absorption) is [25]:

$$P_{abs,int} \approx P_P \Gamma_{gas} \alpha L. \quad (10)$$

Consequently, in MRSI-QEPAS we expect  $p$  to be proportional to the length of absorption  $L$ . The simulation results confirm that the pressure amplitude per input power varies linearly with the absorption length.

As it is possible to see in Fig. 5, the pressure signal obtained in MRSI-QEPAS is one order of magnitude lower than in the MR-QEPAS.

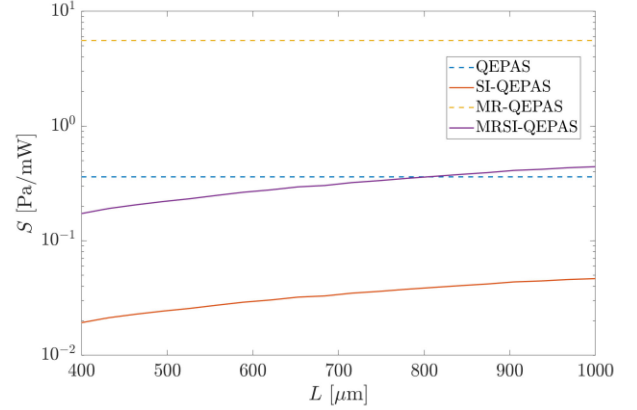


Fig. 5. Pressure signal per input power ( $S$ ) as a function of the length of the waveguide in the SI-QEPAS and MRSI-QEPAS compared to the pressure signal per input power in QEPAS and MR-QEPAS.

However, the guidance of the laser light can be further and more effectively exploited by implementing an optical resonant cavity to be directly coupled with the waveguide modeled and simulated in SI-QEPAS and MRSI-QEPAS configurations.

## V. OPTICAL RESONANT ENHANCEMENT: OMRSI-QEPAS

The results of the previous paragraphs showed that the integrated solutions (SI-QEPAS and MRSI-QEPAS) produce a pressure signal one order of magnitude lower than the corresponding free space configurations (QEPAS and MR-QEPAS).

In order to achieve better performances in terms of signal amplitude with a semi-integrated setup, we propose to implement an optical-resonant-cavity architecture in the MRSI-QEPAS, with the aim of increasing the optical power interacting with the gas target starting from the same input power simulated in the previous configurations. The modification to the MRSI-QEPAS setup is shown in Fig. 1(e). It is possible to see that an optical resonator is fed by an optical bus. The racetrack resonator is designed to have a total length  $L$  and a gap between the two long-side waveguide of  $80 \mu\text{m}$  (bend radius of  $40 \mu\text{m}$ ).

It is easy to demonstrate that the enhancement factor  $E_F$ , calculated as the ratio between the power circulating into a section of the cavity ( $P_{cav}$ ) (modulated at the resonance frequency of the tuning fork) and the input power within the feeding bus ( $P_P$ ) is [26]:

$$E_F = \frac{P_{cav}}{P_P} = \frac{e^{-\alpha_{wg} L} \kappa^2}{\left(1 - e^{-\frac{\alpha_{wg}}{2} L \sqrt{1-\kappa^2}}\right)^2} \approx \frac{4\kappa^2}{(\alpha_{wg} L + \kappa^2)^2} \quad (11)$$

with  $\kappa^2$  the nondimensional power coupling efficiency between a feeding waveguide and the resonator.

In order to estimate the enhancement factor, we considered the propagation loss already estimated (2.7 dB/cm) and bend losses. We estimated the bend losses by evaluating the superposition of the optical mode in the straight waveguide and in the bent waveguide (equal to 99.6%, with a curvature radius of  $40 \mu\text{m}$ ).

$$BL = -4_{interfaces} 10 \log_{10} (0.9966) = 0.013 \text{ dB} \quad (12)$$

TABLE I  
PARAMETERS OF THE OPTICAL RESONATOR

Parameter	Symbol	Value
Cavity length	$L$	1000.63 $\mu\text{m}$
Order of resonance	$m$	488
Resonance wavelength	$\lambda_0$	3.34555 $\mu\text{m}$
Q-factor	$Q$	19749
Finesse	$F$	40.5
Free spectral range (FSR)	FSR	6.86 nm

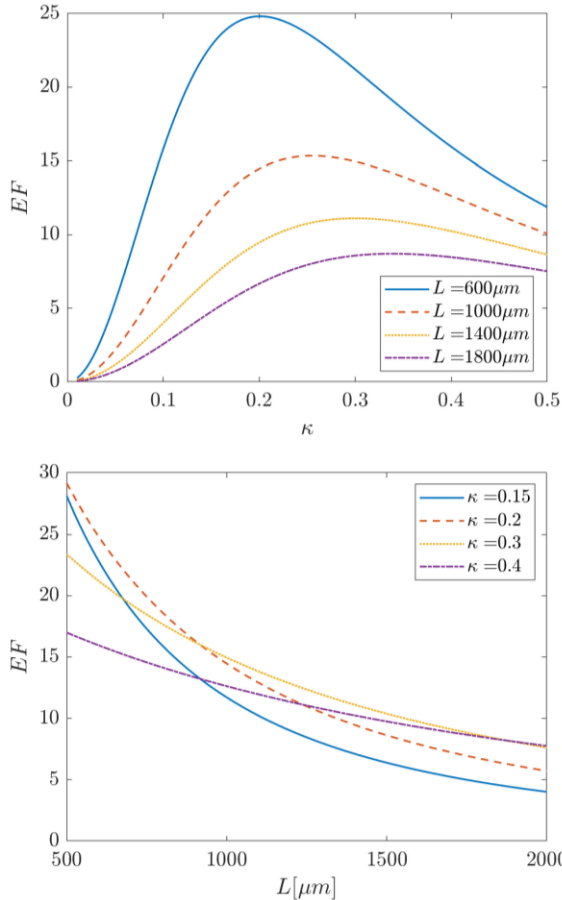


Fig. 6. Enhancement factor as a function of  $\kappa$  for different values of  $L$  (a) and enhancement factor as a function of  $L$  for different values of  $\kappa$ , with estimated loss  $\alpha_{wg} = 0.69$  dB/cm.

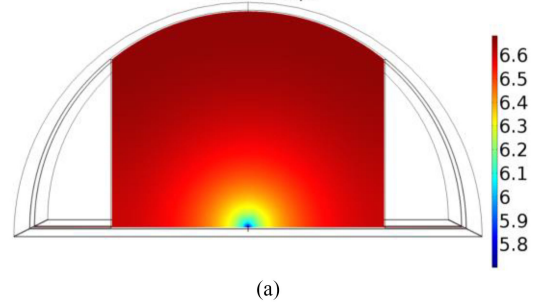
We obtained a bend loss around 0.013 dB per roundtrip (0.013dB/L, with  $L$  the length of the resonator). So,  $\alpha_{wg} = 2.7$  dB/cm + 0.013 dB/L.

The parameters of the final designed resonator are summarized in Table I.

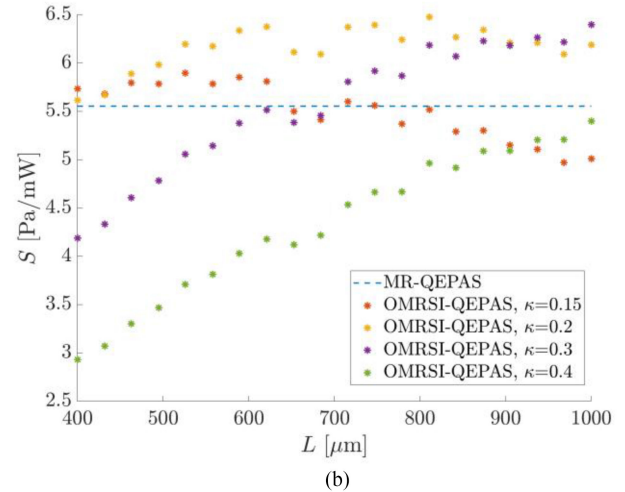
Fig. 6 shows the enhancement factor as a function of the coupling efficiency and the length  $L$  of the resonator.

By properly designing the distance  $d_{gap}$  between the feeding bus and the resonator, the power coupling efficiency  $\kappa^2$  can be calculated end engineered through the following expression

$L=0.001$  m freq(1)=15800 Hz  
Slice: abs(p)



(a)



(b)

Fig. 7. Pressure signal per input power (S) over a central cross section in OMRSI-QEPAS (a) and Pressure signal per input power (S) as a function of the length of the waveguide in OMRSI-QEPAS, compared with MR-QEPAS (b).

(valid for straight couplers) [27]:

$$\kappa^2 = \sin^2 \left( \frac{\pi L_{cp} \Delta n(d_{gap})}{\lambda} \right) \quad (13)$$

Here  $\Delta n(d_{gap})$  is the difference between the effective indices of the even and the odd modes in the coupling region, where the evanescent coupling between feeding bus and resonator takes place.  $L_{cp}$  is the length of the coupling region and  $\lambda$  is the wavelength of input light. Fig. 7(a) shows the pressure amplitude at a central cross section obtained for an optical resonator with a length of  $L = 1$  mm in an OMRSI-QEPAS configuration. Fig. 7(b) shows the performance of the OMRSI-QEPAS as a function of  $L$  at different values of  $\kappa$ , compared with the pressure value obtained with MR-QEPAS. As it can be easily argued from the figure, in an OMRSI-QEPAS configuration comparable or higher-pressure values for the sound wavefront can be achieved with respect to a standard MR-QEPAS approach. Table II summarizes the peak pressure signals obtained for each simulated configuration. The obtained results demonstrate that an integrated configuration of QEPAS (in particular the OMRSI-QEPAS) can exceed the performances of the state-of-art QEPAS configurations. The use of optical enhancement can overcome the problem of a low air confinement factor thanks to the use of optical resonators.

TABLE II  
COMPARISON OF SIGNAL AMPLITUDE FOR DIFFERENT CONFIGURATIONS

Configuration	Peak pressure
SI-QEPAS (1-mm source)	0.047 Pa
FS-QEPAS	0.361 Pa
MRSI-QEPAS (1-mm source)	0.443 Pa
MR-QEPAS	5.55 Pa
OMRSI-QEPAS(1-mm source, $\kappa = 0.3$ )	6.396 Pa

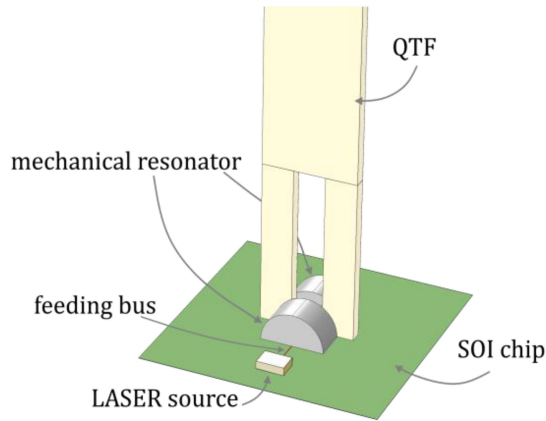


Fig. 8. Final configuration of the OMRSI-QEPAS setup.

Fig. 8 shows the final configuration of the OMRSI-QEPAS setup. Thanks to the possibility of bonding an external laser to a SOI chip, it is possible to feed the optical resonator through a feeding optical bus entering the mechanical resonator. The laser source should be placed sufficiently distant from the mechanical resonator and the QTF to guarantee an effective heat dissipation/cooling and avoid that temperature gradients in the gas affect the photoacoustic generation and response.

As for the fabrication process, the initial step would be to etch the waveguides and the resonator on a standard Si/SiO<sub>2</sub> chip (500 nm of Silicon layer). Then, the external laser would be bonded upon the SOI chip, which can be mounted inside an HHL-like package. As for the mechanical resonator, the simplest approach would be to mechanically bond it to the SOI chip. Finally, the QTF would be connected from the base to the upper enclosure of the packaging and then coupled with the ring resonator upside down. We want to underline that the approach we propose can be extended to other platforms different from Si/SiO<sub>2</sub> (for example on InP platform) where it can be possible to monolithically grow the laser upon the chip.

## VI. CONCLUSION

In this work, we demonstrated that using an integrated chip approach for QEPAS sensing could represent a valid alternative to standard QEPAS, making the sensor smaller and more stable, avoiding any optical alignment and allowing comparable or better performances to be achieved. Despite a limited air

confinement factor of integrated Silicon waveguides for a wavelength of 3.345  $\mu\text{m}$ , the use of a mechanical microresonator and optical resonant enhancement would provide a pressure amplitude higher than the standard free space *on-beam* QEPAS (MR-QEPAS) with the same power consumption. We believe that the proposed device represents a promising solution for miniaturizing the dimensions of a QEPAS sensor, since all the optical parts could be integrated on a chip, except for the quartz tuning fork.

## REFERENCES

- [1] L. B. Kreuzer, "The physics of signal generation and detection," in *Optoacoustic Spectroscopy and Detection*. Amsterdam, Netherlands: Elsevier, 1977, pp. 1–25.
- [2] G. A. West *et al.*, "Photoacoustic spectroscopy," *Rev. Sci. Instrum.*, vol. 54, no. 7, pp. 797–817, 1983.
- [3] P. Patimisco, G. Scamarcio, F. Tittel, and V. Spagnolo, "Quartz-enhanced photoacoustic spectroscopy: A review," *Sensors*, vol. 14, no. 4, pp. 6165–6206, 2014.
- [4] P. Patimisco, A. Sampaolo, L. Dong, F. K. Tittel, and V. Spagnolo, "Recent advances in quartz enhanced photoacoustic sensing," *Appl. Phys. Rev.*, vol. 5, no. 1, 2018, Art. no. 011106.
- [5] P. Patimisco, A. Sampaolo, H. Zheng, L. Dong, F. Tittel, and V. Spagnolo, "Quartz-enhanced photoacoustic spectrophones exploiting custom tuning forks: A review," *Adv. Phys.: X*, vol. 2, no. 1, pp. 169–187, 2016.
- [6] L. Dong, A. Kosterev, D. Thomazy, and F. Tittel, "QEPAS spectrophones: Design, optimization, and performance," *Appl. Phys. B*, vol. 100, no. 3, pp. 627–635, 2010.
- [7] K. Liu, X. Guo, H. Yi, W. Chen, W. Zhang, and X. Gao, "Off-beam quartz-enhanced photoacoustic spectroscopy," *Opt. Lett.*, vol. 34, no. 10, 2009, Art. no. 1594.
- [8] H. Zheng *et al.*, "Application of acoustic micro-resonators in quartz-enhanced photoacoustic spectroscopy for trace gas analysis," *Chem. Phys. Lett.*, vol. 691, pp. 462–472, 2018.
- [9] V. Spagnolo, A. Kosterev, L. Dong, R. Lewicki, and F. Tittel, "NO trace gas sensor based on quartz-enhanced photoacoustic spectroscopy and external cavity quantum cascade laser," *Appl. Phys. B*, vol. 100, no. 1, pp. 125–130, 2010.
- [10] J. Harrington, *Infrared fibers and their applications*. Bellingham, Wash. 1000 20th St. Bellingham WA 98225–6705 USA: SPIE, 2004.
- [11] A. Sampaolo, P. Patimisco, J. Kriesel, F. Tittel, G. Scamarcio, and V. Spagnolo, "Single mode operation with mid-IR hollow fibers in the range 5.1–10.5  $\mu\text{m}$ ," *Opt. Express*, vol. 23, no. 1, pp. 195–204, 2015.
- [12] M. Giglio, P. Patimisco, A. Sampaolo, J. Kriesel, F.K. Tittel, and V. Spagnolo, "Low-loss and single-mode tapered hollow-core waveguides optically coupled with interband and quantum cascade lasers," *Opt. Eng.*, vol. 57, no. 01, 2017.
- [13] A. Sampaolo *et al.*, "Highly sensitive gas leak detector based on a quartz-enhanced photoacoustic SF6 sensor," *Opt. Express*, vol. 24, no. 14, 2016, Art. no. 15872.
- [14] H. Wu *et al.*, "Atmospheric CH<sub>4</sub> measurement near a landfill using an ICL-based QEPAS sensor with V-T relaxation self-calibration," *Sensors Actuators B: Chem.*, vol. 297, 2019, Art. no. 126753.
- [15] Y. Ma, "Review of recent advances in QEPAS-based trace gas sensing," *Appl. Sci.*, vol. 8, no. 10, 2018, Art. no. 1822.
- [16] F. Sgobba *et al.*, "Quartz-enhanced photoacoustic detection of ethane in the near-IR exploiting a highly performant spectrophone," *Appl. Sci.*, vol. 10, no. 7, 2020, Art. no. 2447.
- [17] A. Sampaolo *et al.*, "Quartz-enhanced photoacoustic spectroscopy for hydrocarbon trace gas detection and petroleum exploration," *Fuel*, vol. 277, 2020, Art. no. 118118.
- [18] S. Csutak, W. Li, A. Sampaolo, and G. Ham, "Photoacoustic gas detection," U.S. Patent 10429350B2, Oct. 1, 2019.
- [19] Z. Zhou, B. Yin, and J. Michel, "On-chip light sources for silicon photonics," *Light: Sci. Appl.*, vol. 4, no. 11, pp. e358–e358, 2015.
- [20] V. Passaro, C. Tullio, B. Troia, M. Notte, G. Giannoccaro, and F. Leonardis, "Recent advances in integrated photonic sensors," *Sensors*, vol. 12, no. 11, pp. 15558–15598, 2012.
- [21] Y. Pao, *Optoacoustic Spectroscopy and Detection*. Ed. by Y. Pao. NY, San Francisco, London: Academic, XI, 1977.

- [22] S. Miller *et al.*, “Low-loss silicon platform for broadband mid-infrared photonics,” *Optica*, vol. 4, no. 7, pp. 707–712, 2017.
- [23] L. Rothman *et al.*, “The HITRAN2012 molecular spectroscopic database,” *J. Quantitative Spectrosc. Radiative Transfer*, vol. 130, pp. 4–50, 2013. [Online]. Available: <https://doi.org/10.1016/j.jqsrt.2013.07.002>, Accessed 18 May 2020.
- [24] S. Dello Russo *et al.*, “Acoustic coupling between resonator tubes in quartz-enhanced photoacoustic spectrophones employing a large prong spacing tuning fork,” *Sensors*, vol. 19, no. 19, 2019, Art. no. 4109.
- [25] A. Mason, *Sensing Technology*. Berlin, Germany: Springer, 2016 .
- [26] D. Rabus, *Integrated Ring Resonators*. Berlin, Germany: Springer, 2007.
- [27] H. Nishihara, M. Harupa, and T. Suhara, *Optical Integrated Circuits*. NY, USA: McGraw-Hill, 1989.

**Martino De Carlo** received the master’s degree (*cum laude*) in electronic engineering in 2017 from the Politecnico di Bari, Bari, Italy, where he is currently working toward the Ph.D. degree. He is also a member of the Photonics Research Group. His research interests include the fields of optomechanics and optical sensors. He is the author or coauthor of few papers in international journals.

**Giansergio Menduni** received the M.S. degree (*cum laude*) in electronic engineering in 2017 from the Technical University of Bari, Bari, Italy, where he has been working toward the Ph.D. degree with the Department of Electric and Information Engineering since 2018. His research activity is focused on the development of gas sensors based on quartz enhanced photoacoustic spectroscopy.

**Angelo Sampaolo** received the master’s and Ph.D. degrees in physics from the University of Bari, Bari, Italy, in 2013 and 2017, respectively. He was an Associate Researcher at the Laser Science Group, Rice University from 2014 to 2016 and an Associate Researcher with Shanxi University since 2018. Since May 2017, he was a Postdoctoral Research Associate with the University of Bari and starting from December 2019, he is an Assistant Professor with Polytechnic of Bari. His research activity has included the study of the thermal properties of heterostructured devices via Raman spectroscopy. Most recently, his research interest has focused on the development of innovative techniques in trace gas sensing, based on quartz-enhanced photoacoustic spectroscopy, and covering the full spectral range from near-IR to THz. His achieved results have been acknowledged by a cover paper in *Applied Physics Letters* of the July 2013 issue.

**Francesco De Leonardis** received the Laurea and Ph.D. degrees in electronic engineering from the Politecnico di Bari, Bari, Italy, in 1999 and 2003, respectively. Since 2004, he has been a member of the Photonics Research Group. Since 2018, he has been with Politecnico di Bari as an Associate Professor, for his scientific activities in optoelectronics and photonics. His research interests include mainly the fields of integrated optical sensors and nonlinear photonic devices. He is the author or coauthor of more than 150 papers in international journals and conference presentations, and holds one international patent. He is an Associate Member of the National Institute of Nuclear Physics.

**Vincenzo Spagnolo** received the Ph.D. degree in physics from the University of Bari, Bari, Italy, in 1994. From 1997 to 1999, he was a Researcher at the National Institute of the Physics of Matter. Since 2004, he works with the Technical University of Bari, formerly as an Assistant and Associate Professor, and currently as a Full Professor of Physics. In 2019, he became the Vice-Rector of the Technical University of Bari - Deputy to Technology Transfer. He is the Director of the joint-research lab PolySense between Technical University of Bari and THORLABS GmbH, a Fellow Member of SPIE, and a Senior Member of OSA. His research interests include optoacoustic gas sensing and spectroscopic techniques for real-time monitoring. His research activity is documented by more than 210 publications and three filed patents. He has given more than 50 invited presentations at international conferences and workshops.

**Vittorio M. N. Passaro** (Senior Member, IEEE) received the Laurea degree (*cum laude*) in electronic engineering from the University of Bari, Bari, Italy, in 1988, and the Ph.D. degree in electronic engineering from the Politecnico di Bari, Bari, Italy, in 1992. Since October 2000, he has been with the Politecnico di Bari as an Associate Professor of electronics. Since 2004, he has been the Founder and the Leader of the Photonics Research Group, Politecnico di Bari. He is the author or coauthor of more than 400 papers in optoelectronics and photonics topics, published in international journals (one by *Nature Photonics*) and conference proceedings. He holds two international patents and is the Editor of five scientific books (one by Springer). He is a Senior Member of the Optical Society of America and an Associate Member of the National Institute of Nuclear Physics.